

Search for Neutron-Antineutron Oscillations Using Multiprong Events in Soudan 2

J. Chung⁵, W.W.M. Allison³, G.J. Alner⁴, D.S. Ayres¹, W.L. Barrett⁶,
P.M. Border², J.H. Cobb³, H. Courant², D.M. Demuth²
T.H. Fields¹, H.R. Gallagher⁵, M.C. Goodman¹, R. Gran²,
T. Joffe-Minor¹, T. Kafka⁵, S.M.S. Kasahara², P.J. Litchfield⁴,
W.A. Mann⁵, M.L. Marshak², R.H. Milburn⁵, W.H. Miller², L. Mualem²,
A. Napier⁵, W.P. Oliver⁵, G.F. Pearce⁴, E.A. Peterson², D.A. Petyt⁴,
K. Ruddick², M. Sanchez⁵, J. Schneps⁵, A. Sousa⁵,
B. Speakman², J.L. Thron¹, S.P. Wakely², N. West³

¹*Argonne National Laboratory, Argonne, IL 60439*

²*University of Minnesota, Minneapolis, MN 55455*

³*Department of Physics, University of Oxford, Oxford OX1 3RH, UK*

⁴*Rutherford Appleton Laboratory, Chilton, Didcot, Oxfordshire OX11 0QX, UK*

⁵*Tufts University, Medford, MA 02155*

⁶*Western Washington University, Bellingham, WA 98225*

November 12, 2018

Abstract

We have searched for neutron-antineutron oscillations using the 5.56 fiducial kiloton-year exposure of the Soudan 2 iron tracking calorimeter. We require candidate $n\bar{n}$ occurrences to have ≥ 4 prongs (tracks and showers) and to have kinematics compatible with $n\bar{n}$ annihilation within a nucleus. We observe five candidate events, with an estimated background from atmospheric neutrino and cosmic ray induced events of 4.5 ± 1.2 events. Previous experiments with smaller exposures observed no candidates, with estimated background rates similar to this experiment. We set a lifetime lower limit at 90% CL for the $n\bar{n}$ oscillation time in iron: $T_A(Fe) > 7.2 \times 10^{31}$ years. The corresponding lower limit for oscillation of free neutrons is $\tau_{n\bar{n}} > 1.3 \times 10^8$ seconds.

PACS numbers: 11.30.Fs, 12.20.Fv, 12.60.Jv, 14.20.Dh

1 Introduction

1.1 Neutron-antineutron oscillations

An intriguing variation on the grand unification theme that nucleons are likely to be unstable is the proposal that neutrons can oscillate into antineutrons. Neutron-antineutron oscillations were first predicted in 1970 by V. A. Kuzmin in a model intended as a realization of requirements given earlier by A.D. Sakharov for evolution of the universe to net baryon asymmetry [1, 2]. Subsequently $n\bar{n}$ oscillations emerged as a predicted reaction in certain grand unification theories [3]. More recently it has been shown that $n\bar{n}$ oscillations can occur in a large class of supersymmetric $SU(2)_L \times SU(2)_R \times SU(4)_c$ models [4]. In such models the dominant baryon number violating process is a $\Delta B = -2, \Delta L = 0$ nucleon transition (e.g. $n\bar{n}$ oscillations or $p + n \rightarrow$ pions) rather than a $\Delta B = -1, \Delta L = -1$ nucleon-antilepton transition (e.g. $p \rightarrow e^+\pi^0$ or $p \rightarrow \bar{\nu}K^+$). Neutron-antineutron oscillations have also been indicated as viable by recent GUT models which invoke the existence of extra spacetime dimensions [5].

If indeed a neutron can evolve into an antineutron, the experimental signatures for the metamorphosis should be distinctive. The resulting antineutron will annihilate with a baryon of the surrounding environment, producing multiple mesons ($B = 0$) whose visible energy and net momentum are approximately those of two nucleon masses having nuclear Fermi motion.

From the phenomenology of neutron-antineutron oscillations it can be shown [6] that the oscillation time T_A of a neutron bound within a nucleus of atomic mass A is related to the neutron oscillation time in vacuum $\tau_{n\bar{n}}$ according to

$$T_A = (\tau_{n\bar{n}})^2 \cdot T_R. \tag{1}$$

Here T_R , which has units of inverse time, is the suppression factor representing the effect of the nuclear environment which substantially prolongs the effective oscillation time.

Detailed calculations of the suppression factor T_R for parent nuclei of experimental interest, including deuterium, oxygen, argon, and iron, have been reported in literature. The calculations utilize phenomenological frameworks provided by nuclear potential theory [7, 8], and by S-matrix theory [9, 10, 11, 12]. In the analysis of Dover, Gal, and Richard [7], it is proposed that neutron-antineutron oscillations will occur mostly in outer nuclear shells and near the nuclear surface. However reservations concerning this picture have been expressed and in a number of calculations the entire nuclear volume contributes to $n\bar{n}$ oscillations [8].

1.2 Previous experimental searches

Two types of experiments have been used to search for neutron-antineutron oscillations. In one approach, slow neutrons from a fission reactor are channeled through a magnetically shielded vacuum pipe towards a target region. An antineutron produced during the flight will annihilate in the target and the annihilation products are registered by detectors surrounding the target. Experiments of this type have been carried out at Pavia [13] and at Grenoble

[14, 15]. The Grenoble reactor experiment obtained $\tau_{n\bar{n}} \geq 0.86 \times 10^8$ s at 90% confidence level (CL). This is the most stringent oscillation time lower limit reported to date using free neutrons.

The alternate approach, used in this experiment, is to continuously monitor neutrons bound in nuclei, usually as part of an ongoing nucleon decay search. Searches of this type have been reported by the underground experiments Homestake [16], NUSEX [17], KOLAR [18], IMB [19], Kamiokande [20], and Fréjus [21]. The searches by Kamiokande and Fréjus obtained the most stringent $n\bar{n}$ oscillation time lower limits.

In a search based upon a 1.11 kiloton-year (kty) exposure of the Kamiokande-I water Cherenkov detector [20], no candidate $\bar{n}N$ event was observed. An oscillation time lower limit of $T_A > 4.3 \times 10^{31}$ years at 90% CL was set. Using the suppression factor $T_R = 1 \times 10^{23}$ s⁻¹ calculated by Dover *et al.* for oxygen [7], Kamiokande obtained an oscillation time limit for free neutrons of $\tau_{n\bar{n}} > 1.2 \times 10^8$ seconds at 90% CL. The Fréjus collaboration, in a search using a 1.56 fiducial kty exposure of the experiment's planar iron tracking calorimeter, also reported zero $n\bar{n}$ oscillation candidates. The oscillation time lower limit for T_A in iron thereby obtained was 6.5×10^{31} years at 90% CL. Using $T_R = 1.4 \times 10^{23}$ s⁻¹ as calculated by Dover *et al.* for iron, Fréjus determined the free neutron limit to be also $\tau_{n\bar{n}} > 1.2 \times 10^8$ seconds at 90% CL [21].

In the Kamiokande analysis an enhanced probability for $n\bar{n}$ oscillations to occur in the nuclear periphery as postulated by Dover *et al.* was assumed. In the Monte Carlo simulations of the experiment, the effect of this assumption is to reduce distortion of the final state meson spectrum arising from intranuclear absorption and inelastic scattering processes. As a result experimental detection efficiencies are enhanced relative to expectations for the case where oscillations may occur throughout the entire volume of parent nuclei. The search reported here follows the more conservative approach adopted previously by Fréjus. For our primary $\bar{n}N$ simulation on which our detection efficiency is based, we assume $n\bar{n}$ oscillation to occur throughout the nuclear volume. However the effects of peripheral predominance are also described.

2 Detecting $n\bar{n}$ Oscillations in Soudan 2

2.1 Detector and data exposure

Soudan 2 is a 963 metric ton (770 tons fiducial) iron tracking calorimeter of honeycomb lattice geometry which operates as a slow-drift time projection chamber [22]. The tracking elements are one-meter-long drift tubes filled with an Argon-CO₂ gas mixture. Electrons liberated by throughgoing charged particles drift to the tube ends under the action of a voltage gradient applied along the tubes. The drift charge is registered by vertical anode wires, while horizontal cathode pad strips register the image charges. The third coordinate is obtained from the drift-time. The amount of charge measures the deposited ionization. The drift tubes are laid onto corrugated steel sheets, and the sheets are stacked to form 1×1×2.5 m, 4.3 ton modules from which the calorimeter is assembled in building-block

fashion. Surrounding the tracking calorimeter on all sides but mounted on the cavern walls and well separated from calorimeter surfaces is a 1700 m² active shield array of two or three layers of proportional tubes [23]. The shield facilitates identification of events which are not contained within the calorimeter. In particular, it provides tagging of background events initiated by cosmic-ray-induced neutrons.

The detector is located at a depth of 2070 meters–water–equivalent on the 27th level of the Soudan Underground Mine State Park in northern Minnesota. The modular design enabled data taking to commence in April 1989 when the detector was one-quarter of its final size; routine operation with the fully–deployed detector got underway in November 1993. The fiducial (total) exposure analyzed here, obtained from data–taking through December 2000, is 5.56 (6.96) kiloton–years.

Calibration of calorimeter module response was carried out at the Rutherford ISIS spallation neutron facility using test beams of positive and negative pions, electrons, muons, and protons [24]. Spatial resolutions for track reconstruction and for vertex placement in anode, cathode, and drift time coordinates are of the same scale as the drift tube radii, ≈ 0.7 cm. In Soudan 2, ionizing particles having non-relativistic as well as relativistic momenta are imaged with dE/dx sampling in a fine–grained honeycomb lattice geometry. Protons can be distinguished from pions and muons via ionization and ranging, energetic muons discriminated from pions via absence of secondary scatters, and prompt e^\pm showers distinguished from photon showers on basis of proximity to primary vertices. These event imaging capabilities offer advantages, in comparison to water Cherenkov detectors and to planar iron calorimeters, for analysis of the complicated multiprong topologies that would arise with $\bar{n}N$ annihilations initiated by $n\bar{n}$ oscillations.

2.2 Simulation of $\bar{n}N$ annihilation arising from $n\bar{n}$ oscillations

We have developed realistic simulations of $n\bar{n}$ oscillations yielding $\bar{n}N$ annihilations as they would occur in the iron nuclei which comprise the bulk of the calorimeter mass. Generation of $\bar{n}N$ events is carried out as follows:

Momenta of the initial state antineutron and nucleon are assigned according to a distribution based upon a Fermi-gas model parameterization of quasi-elastic electron nucleus scattering [25]. Final state particle four-momenta were constructed in accordance with N-body phase space [26]. Assignment of $\bar{n}N$ reactions to generated events is weighted according to cross section data for $\bar{p}p$ annihilation at rest [27, 28]. For the purpose of channel selection, $\bar{n}n$ annihilations are assigned the same cross sections as observed for $\bar{p}p$; $\bar{n}p$ is assumed to have the same total rate as $\bar{p}p$, and cross sections were inferred from $\bar{p}p$ as allowed by charge conservation. We restricted our reaction compilation to cross sections exceeding 2% of the total $\bar{N}N$ cross section. Consequently production of ρ , ω , charged and neutral pions and kaons is represented, however final states with η and η' mesons were neglected.

Provision was made to include intranuclear rescattering (INS) of final state pions in the simulations. Our treatment follows the approach utilized previously in simulations of atmospheric neutrinos and of nucleon decay [24]. Pions, either directly produced in annihilation or in ρ decays, are propagated through a model nucleus. The nuclear radius and density are

parameters of the model; the radius is scaled according to $A^{1/3}$. Scattering in the nuclear medium is characterized using a momentum-dependent pion interaction length. The nuclear parameters were set by requiring the model to reproduce single and multiple pion production rates observed in bubble chamber ν_μ -deuteron ($A=2$) and ν_μ -neon ($A=20$) interactions [29]. For pions from vertices placed at random within an iron nucleus, our model predicts $\sim 45\%$ to emerge either unscattered or to have undergone only small angle elastic scattering. About 30% are predicted to undergo total absorption, while the remainder undergo charge exchange (9%) or emerge having undergone inelastic scattering (16%). Our treatment of nuclear rescattering does not include proton secondaries. While it is expected that protons would occasionally be ejected from parent nuclei as the result of rescattering, their momenta would almost always fall below the effective threshold (approx. 450 MeV/ c) for creation of distinct tracks in the detector.

For simulations with intranuclear rescattering included, the average multiplicity per event for mesons emerging from an iron nucleus is 3.8 with rms deviation 1.2. The average track plus shower multiplicity emitted from an iron nucleus (“prong multiplicity”) per event is 5.0 with an rms deviation of 2.1 prongs. (Note these multiplicities are for “perfect detection”.)

The $\bar{n}N$ event generation produces four-momenta of all particles which exit the parent nuclei. This information is fed, event-by-event, into the Soudan 2 Monte Carlo (MC) which provides a realistic detector response. The simulation includes detector background “noise” arising from natural radioactivity and from the electronics. Event records are generated with format identical to that of data events, allowing $n\bar{n}$ oscillation events to be processed using the same codes and procedures as for data and for events of the atmospheric neutrino Monte Carlo.

2.3 Properties of processed $\bar{n}N$ samples

Three separate $\bar{n}N$ simulation samples were generated. For each sample, events were generated at random locations throughout the tracking calorimeter as it evolved during the experiment’s eleven years of data-taking. In our “primary” simulation, $\bar{n}N$ annihilations were started at random points throughout their parent nuclei and pion intranuclear rescattering was implemented. In a second simulation which also included intranuclear rescattering, $\bar{n}N$ annihilations were restricted to the nuclear periphery ($0.75R \leq r \leq R$, where R is the nuclear radius). A third simulation was carried out in which no pion intranuclear rescattering was included.

Each of the three oscillation samples was processed using a sequence of selections and procedures very similar to that routinely used in reduction of data events in Soudan 2. Each sample was subjected (in software) to the hardware trigger. Events which passed the hardware trigger requirements were subjected to two different software “Filter” codes. The Filters impose event containment criteria, e.g. that no track from the event approaches closer than 20 cm to the detector outer surfaces; they also mitigate against backgrounds arising from cosmic ray muons, natural radioactivity, and detector noise. Events which survived the Filters were then subjected to two separate scans by physicists. Scanning was carried out using interactive color graphics workstations. The scan rules provided refinements to the

Filter selections and introduced requirements on imaging quality, e.g. an event was rejected if (i) its primary vertex occurred in material interior to the detector but not instrumented, or if (ii) its proximity to inter-module gaps compromised the reconstruction of the event.

Events which survived successive application of the hardware trigger, software filters, and physicists’ scans are tallied in the upper four rows of Table 1 for each of the three simulations. These entries are input to the calculation of the detection efficiency for neutron-antineutron oscillations in Soudan 2 as will be described in Sect. 5.

<i>Event Processing and Selection Stages</i>	$\bar{n}N$ annihilation without INS	$\bar{n}N$ annihilation in nuclear periphery with INS	$\bar{n}N$ annihilation in nuclear volume with INS
Initial sample	491	491	491
Hardware trigger	490	469	451
Containment and quality filters	288	301	286
Two physicist scans	214	229	205
Multiplicity ≥ 4 ; no proton events	172	148	135
Exclude events with “muons”	146	130	123
Kinematic selection on $E_{vis}, P/E$	137	102	86

Table 1: Survival through successive processing and selection stages for events of three different simulations of $\bar{n}n$ oscillations yielding $\bar{n}N$ annihilations in Soudan 2.

Preliminary to kinematic reconstruction, the topology of each event was characterized in terms of track and shower prongs. A track prong results when an ionizing, non-showering charged particle (e.g. a pion, muon, or proton) traverses drift tubes of the calorimeter’s honeycomb lattice leaving a continuous trail of tube “hits”. A shower prong on the other hand is created by photon conversion or by a primary electron or positron. The electromagnetic shower consists of many distinct particles and exhibits a cone-like pattern of hits, interspersed with gaps, which is aligned with the direction of the initiating photon or electron. The mean conversion length for photons in Soudan 2 is approximately 15 cm. As a consequence, photon-induced showers generally appear in the vicinity of but moderately displaced from event primary vertices.

Images of two $\bar{n}n$ oscillation events simulated with full detector response are displayed in Fig. 1, where the anode (X) versus drift time (Z) view of each event is shown. For event scanning, three views are always used, including cathode-time and anode-cathode as well as anode-time projections. (The anode-cathode view is automatically assembled for all events, MC as well as data, using demultiplexing and hit-matching algorithms.) As suggested by Fig. 1, $\bar{n}N$ events appear to be energetic yet isotropic to a degree uncommon for data events and for events of the atmospheric neutrino Monte Carlo.

The occurrence of relatively high multiplicity per event of track plus shower prongs is a signature feature of $\bar{n}N$ annihilation. From simulation of $\bar{n}n$ oscillation events in the absence of intranuclear rescattering, we find the prong multiplicity distribution - after triggering, filtering, scanning, and reconstruction - to have a mean of 6.3 prongs per event with an rms width of 2.8 prongs. Here the prong multiplicity is relatively high (compared to multiplicities as generated, see Sect. 2.2), due to depletion of low multiplicities by the processing. With

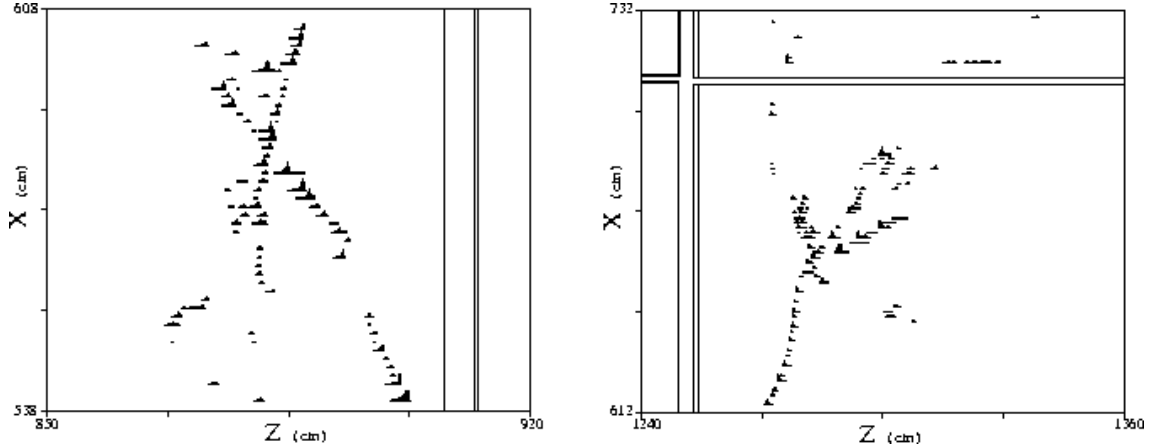


Figure 1: Anode versus drift time views (magnified) of two simulated annihilation events within iron nuclei following $\bar{n}\bar{n}$ oscillation. The multiprong hadronic final states of these events are isotropic to a degree unusual for neutrino interactions.

intranuclear rescattering included, the prong multiplicity distributions of processed samples are shifted lower. For both simulations with INS included, the multiplicity distributions have mean values of 4.8 prongs with rms widths of 3.2 prongs. Thus a sizable contribution from multiplicities exceeding three-prongs survives in the latter simulations. Events of this kind are relatively uncommon among contained atmospheric neutrino events.

In addition to event topology, the reconstructed kinematic quantities E_{vis} , the visible energy, and P_{net} , the net momentum, provide discrimination between $\bar{n}\bar{N}$ and background events. These quantities and their correlation have been used previously in our searches for nucleon decay [30]. E_{vis} is calculated as the sum of the relativistic energies for each of the final state tracks (using the pion mass) and showers. There occur a few short, heavily ionizing tracks which satisfy our identification criteria for protons [31]. For these, only the kinetic energy is added into the calculation of E_{vis} . Distributions of E_{vis} versus P_{net} for $\bar{n}\bar{N}$ events in the absence of and including intranuclear rescattering, are plotted in Fig. 2a and Fig. 2b respectively. Reconstructed events, even in the absence of INS as in Fig. 2a, exhibit large energy losses arising from low energy prongs and secondary hadronic scatters which are unresolved. Consequently the events cluster well below E_{vis} of 1.88 GeV. Comparison of Fig. 2a with Fig. 2b shows that a further large degradation arises with INS. The INS effects substantially increase the kinematic overlap of $\bar{n}\bar{N}$ events with atmospheric neutrino events.

3 Data and Backgrounds for the $\bar{n}\bar{N}$ Search

3.1 Neutrino, rock, and atmospheric ν MC events

Since $\bar{n}\bar{N}$ events generally have high multiplicities we restrict our analysis to events having a “multiprong” topology, that is, having two or more produced particles emerging from primary vertices. Quasi-elastic neutrino interactions which produce a charged lepton plus

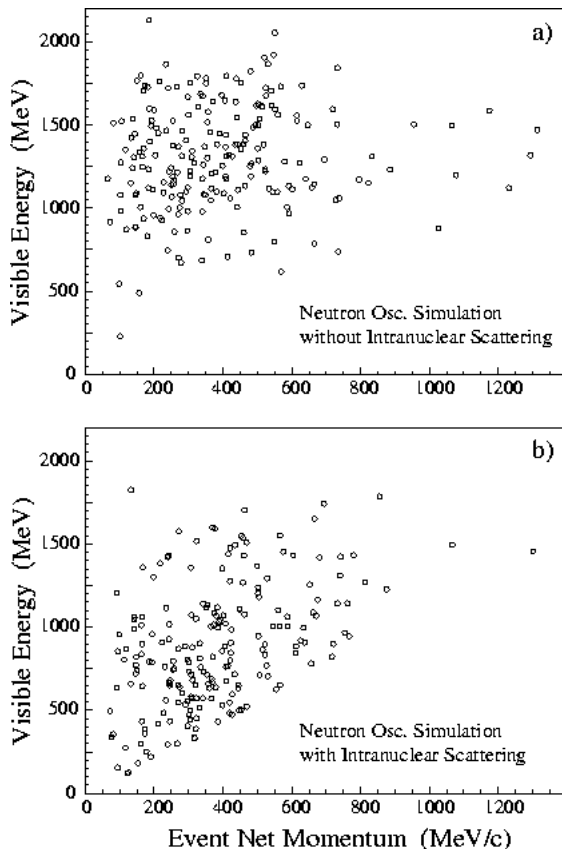


Figure 2: Distributions of visible energy versus magnitude of vector net momentum for reconstructed $\bar{n}N$ annihilation events of two independent full detector simulations. The simulation plotted in 2a (2b) omits (includes) intranuclear rescattering of final state pions. The shift to lower E_{vis} in simulation of b) versus a) arises from pion absorption and inelastic scattering within iron nuclei.

a recoil proton are readily distinguished and removed. As was done for the simulated $n\bar{n}$ events, we require all events under consideration to be fully contained in an interior volume which is everywhere 20 cm from calorimeter outer surfaces.

Three multiprong event samples, which are in addition to the simulated $n\bar{n}$ samples discussed above, have been isolated for this search:

First and foremost are data events for which the cavern-liner active shield array was quiescent during the allowed time window. These events comprise our *shield-quiet data sample*. They originate mostly with atmospheric neutrino interactions but would also include $n\bar{n}$ oscillation events. There are 188 multiprong events in the shield-quiet data of this analysis.

There is a second category of data events which comprises a background to neutrino multiprongs as well as to $n\bar{n}$ oscillations. Events of this category are usually produced by energetic neutrons released in inelastic cosmic ray muon interactions with the cavern rock surrounding the tracking calorimeter. Most of these *rock events* are accompanied by charged particles which give coincident hits in the active shield array; they constitute our *shield-tagged*

rock event sample. However, a few rock events are not accompanied by shield hits, either because of shield inefficiency (detection efficiency is 94%) or because no charged particles enter the cavern along with a rock neutron. The latter *shield-quiet rock events* may end up as background in shield-quiet data. Fortunately the shield-tagged rock events provide a control sample from which the amount of residual rock background in shield-quiet data may be inferred.

The predominant background for $n\bar{n}$ oscillations arises from the atmospheric neutrino reactions. Their contribution is evaluated using the Soudan 2 *atmospheric neutrino Monte Carlo sample*. Our neutrino MC simulation utilizes the atmospheric flux calculation of the Bartol group for the Soudan site [32]. Details of the neutrino event generation and comparisons with low energy νN data are given elsewhere [33]. MC atmospheric neutrino events were inserted into the experiment’s data stream during data-taking. The MC events were introduced at a rate 6.06 times higher than the data rate expected (for null neutrino oscillations) from the atmospheric neutrino flux. The events were processed identically to real data events, with their identity revealed only at the final analysis stage. The atmospheric ν MC multiprong sample finally extracted contains 1267 events.

Properties of our multiprong data, rock, and neutrino MC samples germane to an $n\bar{n}$ oscillation search are reported below. Further details can be found in previous publications [24, 30, 31].

3.2 Multiprong data compared to atmospheric ν MC

The prong multiplicity distribution of the shield-quiet data sample is summarized using tallies in the grid displayed in Table 2. In the Table, the topology of each event is represented by the number of tracks, n_{track} , and number of showers, n_{shower} , which comprise the visible final state. The number of data events which have a particular (n_{track}, n_{shower}) combination are given by the upper entries at the grid location having the appropriate integer coordinates. The multiprong data topologies having highest rates are seen to be combinations of lowest multiplicity, namely $(n_{track}, n_{shower}) = (2, 0)$ and $(1, 1)$. For comparison, the corresponding prong distribution for the atmospheric neutrino MC event sample is given by the lower entries in each of the track-shower grid locations of Table 2. The MC sample (for null neutrino oscillations) has been normalized to the same fiducial exposure as for the data ($1267/6.06 = 209.1$ events). The two distributions are seen to match well, e.g. the χ^2/bin averages to below 1.0, with the exception of the $(1, 2)$ topology. Since most shield-quiet data multiprongs are initiated by atmospheric neutrinos, the agreement is evidence that the neutrino MC provides a good general representation of our data.

Kinematics for the shield-quiet multiprong data is shown by the E_{vis} versus vector net momentum diplot of Fig. 3a. The events populate a broad, correlated region extending from threshold to 1.5 GeV (1.5 GeV/ c) in visible energy (net momentum). Portions of this data distribution overlap the distribution predicted for $n\bar{n}$ events shown in Fig. 2b.

A direct comparison with kinematics for the atmospheric neutrino MC sample is provided by Fig. 3b. Note that the latter sample has an exposure-equivalent of 33.7 fiducial kton-years. The distribution of the MC sample, normalized to the exposure, is very similar to

Number of Tracks								
5	<i>Data</i>	0	0	0	2	1	1	
	<i>MC</i>	0.3	0.3	0.3	0	0.2	0.5	
4	<i>Data</i>	3	1	3	0	1	0	
	<i>MC</i>	2.1	0.3	0.2	1.6	0.2	0.2	
3	<i>Data</i>	16	7	2	2	0	0	
	<i>MC</i>	14.5	5.1	3.1	1.4	1.6	0.3	
2	<i>Data</i>	26	20	15	4	0	2	
	<i>MC</i>	26.8	21.1	14.6	5.9	2.7	1.3	
1	<i>Data</i>		25	10	5	3	3	
	<i>MC</i>		28.3	23.6	9.3	5.0	1.6	
0	<i>Data</i>			14	13	4	1	
	<i>MC</i>			12.4	9.0	2.9	2.1	
		0	1	2	3	4	5	Number of Showers

Table 2: Event topology distributions: Event counts are tabulated according to (n_{track}, n_{shower}) combination per event, for multiprongs events of the data sample (upper entries) and of the atmospheric neutrino MC sample (lower entries). Event tallies of the latter sample represent expectations for an atmospheric flux with null ν_μ oscillations normalized (factor of 6.06) to the data exposure.

that of the data.

In Fig. 3, events which have prompt protons are denoted by solid circles. As previously noted, such events are highly improbable as $n\bar{n}$ oscillations. However our atmospheric ν MC indicates that detectable recoil protons are to be expected in 24% of neutrino multiprongs, and this expectation is born out by the frequency of recoil proton events observed in the data of Fig. 3a. In Fig. 3a there is a tendency for data events having recoil protons to occur in a region parallel to and below the more populated kinematic band. This trend is reproduced in the MC distribution of Fig. 3b.

3.3 Background from rock events

Rock data events which are flagged by hits in the surrounding shield array, have a distribution of vertex depth into the detector which reflects the mean hadronic interaction length of neutrons in the Soudan detector medium, approximately 80 cm. A rock background component in our shield-quiet multiprongs data will have a corresponding vertex depth distribution in the detector. Neutrino and $n\bar{n}$ oscillation events on the other hand, will distribute uniformly throughout the detector volume. Thus by fitting the distribution of vertex depths observed in our multiprongs data to the sum of two component distributions representing vertex depths of shield-tagged rock and of neutrino MC events, the amount of shield-quiet rock contamination can be determined [31]. On the basis of a maximum likelihood fit, we estimate

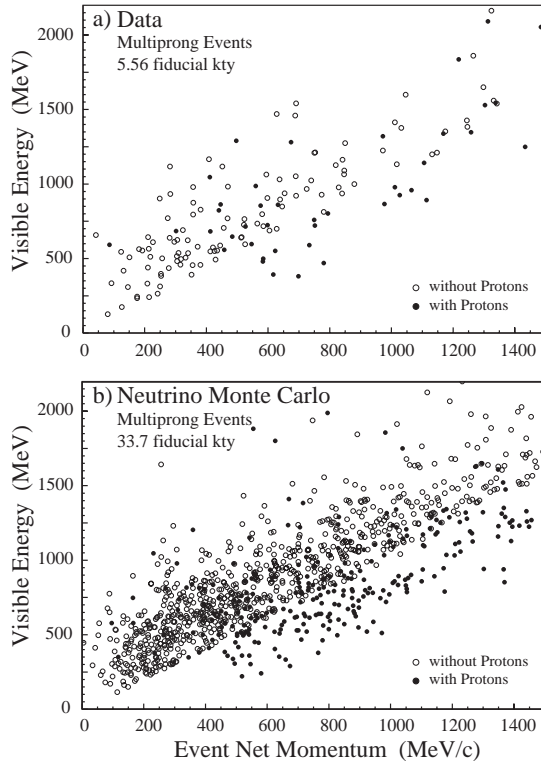


Figure 3: E_{vis} versus P_{net} distributions for shield-quiet data events and for events of the atmospheric neutrino MC sample. Events without (with) proton tracks are depicted using open (solid) circles. The ν MC sample (3a), which corresponds to an exposure (for null ν oscillations) of 6.06 times the data, reproduces the general kinematic trends of multiprongs data (3b).

that a fraction $0.06^{+0.11}_{-0.06}$ of shield-quiet data multiprongs are produced by rock neutrons.

4 Selection of $n\bar{n}$ Oscillation Events

Four selection criteria for neutron oscillation candidates (Table 3) have been defined and applied to all event samples. The selections are designed to maximize $n\bar{n}$ detection in the shield-quiet multiprongs data sample while minimizing backgrounds, the principal one arising from inelastic interactions of atmospheric neutrinos.

<i>Cut</i>	<i>Definition</i>
1.	$N_{prong} \geq 4$
2.	No prompt “proton” tracks
3.	No prompt “muon” tracks longer than 150 cm
4.	Evt kinematics: $P/E < 0.6, 700 < E_{vis} < 1800$ MeV

Table 3: Selection cuts for $n\bar{n}$ oscillation events in Soudan 2.

1. *Prong multiplicity:* We require the sum of track and shower prongs directly associated with the primary vertices to be greater than or equal to four. This value is below but near to the mean multiplicities for processed $n\bar{n}$ samples as discussed in Sect. 2.3. Lowering our selection to include three-prongs would increase the efficiency for $\bar{n}N$ detection by only 3%, however backgrounds arising from atmospheric neutrinos and rock events would increase by 21% and 32% respectively.
2. *Primary proton tracks:* Events having proton tracks emerging from their primary vertices are removed from consideration as $n\bar{n}$ oscillation candidates. The rate of prompt protons is negligible for $\bar{n}N$ annihilation events, however $\sim 24\%$ of atmospheric neutrino events and $\sim 33\%$ of rock events have visible recoil protons.
3. *Primary muon tracks:* Pions produced in $\bar{n}N$ annihilations usually scatter, become absorbed, or range-to-stopping over distances comparable to the calorimeter's hadronic interaction length of 80 cm. In order to mitigate against ν_μ charged current background, we regard any non-scattering track which has pion/muon ionization and range-to-stopping ≥ 150 cm (240 g/cm²) to be a muon track. Any event having such a track is rejected. This selection eliminates 36% of the atmospheric neutrino sample while cutting less than 10% of $n\bar{n}$ events of the primary simulation.
4. *Event kinematics:* As our final criterion we require the kinematics of $n\bar{n}$ candidates to be compatible with those of $\bar{n}N$ annihilation. The event net momentum fraction P_{net}/E_{vis} (hereafter P/E) has previously been shown to be a useful variable for separating $n\bar{n}$ oscillation events from atmospheric neutrino reactions [21], and its utility is confirmed in our analysis. Figures 4a and 4b show P/E versus E_{vis} for $\bar{n}N$ events after topology cuts (1 through 3) from simulations in which oscillations occur throughout the parent nuclear volumes. For the case of no intranuclear rescattering (Fig. 4a), approximately 94% of $n\bar{n}$ oscillation events occur in a region having P/E less than 0.6, with E_{vis} ranging from one to two nucleon masses. With intranuclear rescattering included, Fig. 4b, the $n\bar{n}$ event population shifts to lower values of E_{vis} and to higher values of P/E . Nevertheless a degree of clustering remains which allows a useful search region in the $(E_{vis}, P/E)$ plane to be defined. Our selection for $n\bar{n}$ kinematics is depicted by the rectangular region (dotted-line boundary) shown in the Figs 4-6. Candidate $n\bar{n}$ events are required to have $P/E < 0.6$ and $700 < E_{vis} < 1800$ MeV. These cuts are designed to minimize the atmospheric neutrino background shown in Fig. 5 while maximizing the acceptance for $\bar{n}N$ events.

5 $n\bar{n}$ Candidates and Backgrounds

The reductions in each $\bar{n}N$ annihilation sample upon successive $n\bar{n}$ candidate selections are summarized in the bottom three rows of Table 1. It can be seen that intranuclear rescattering

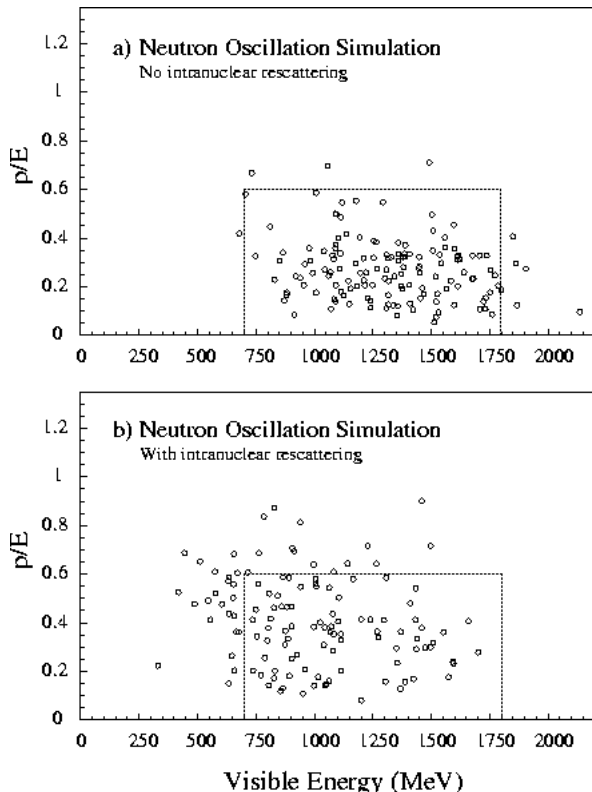


Figure 4: Momentum fraction versus visible energy for events from $n\bar{n}$ simulation after topology cuts, with intranuclear rescattering omitted (4a) versus included (4b). The kinematic search region of this experiment enclosed by the dotted-line boundary, contains 94% of events which pass topology selections. In the more realistic simulation of 4b however, INS degrades E_{vis} and increases momentum anisotropy on average, leaving 70% of events in the search region.

significantly lowers the survival rates. For our primary simulation, with INS operative and with annihilations occurring throughout the volume of the parent nucleus, 86 events from an initial 491 event sample survive all selections, giving a detection efficiency of 0.18 ± 0.02 . Detection efficiencies for the comparison simulations are higher, $(28 \pm 3)\%$ for the simulation without INS, and $(21 \pm 2)\%$ for the simulation which includes INS but restricts annihilations to the nuclear periphery.

Shield-quiet data events which satisfy $n\bar{n}$ selections 1–3 of Table 3 distribute in the P/E versus E_{vis} plane as shown in Fig. 6. Of these sixteen events, five occur within the kinematically allowed region and are candidate $n\bar{n}$ oscillation events of this search. Three of the candidates have four-prong topologies, while the remaining two are five-prong events.

Two views of one of the candidates consisting of four pion-or-muon tracks emerging cleanly from a reaction vertex, are shown in Fig. 7. This event is also consistent with multipion production by atmospheric neutrinos, e.g. $(\bar{\nu}) + n \rightarrow \mu^{\pm} \pi^{\mp} \pi^+ \pi^- (N)$ [34].

Fig. 5 shows that, among atmospheric ν MC events which satisfy topology selections 1–3 of Table 3, there are 28 events (11 ν_{μ} CC, 7 ν_e CC, and 10 NC) which occur in the

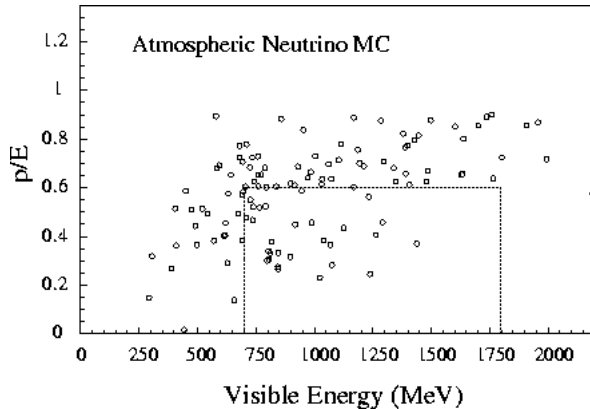


Figure 5: Kinematic distribution of atmospheric neutrino MC events which survive topology selections for $n\bar{n}$ candidates. Events which occur within the bordered region represent the background expected from an exposure (assuming null neutrino oscillations) which is 6.06 times the data exposure.

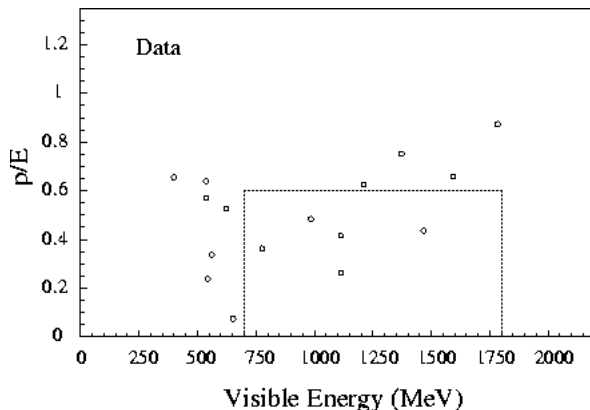


Figure 6: Distribution of data multiprong events after topology selections, in the P/E_{vis} versus E_{vis} plane. Five events are observed to have kinematics compatible with $n\bar{n}$ oscillations in the Soudan 2 detector.

selected kinematic region. That is, 28 neutrino-induced background events would occur in a 33.7 fiducial kiloton-year exposure to an atmospheric neutrino flux having null neutrino oscillations. However strong evidence for atmospheric neutrino oscillations now exists [35], [36], [31, 37]. We allow for neutrino oscillations in our background estimate by weighting our MC ν_μ CC prediction by the atmospheric neutrino flavor ratio-of-ratios: $R_\nu = [(\nu_\mu + \bar{\nu}_\mu)/(\nu_e + \bar{\nu}_e)]_{Data}/[(\nu_\mu + \bar{\nu}_\mu)/(\nu_e + \bar{\nu}_e)]_{MC}$. We have used the value of R_ν measured in this experiment, based upon a 5.14 fiducial kton-year exposure: $R_\nu = 0.68 \pm 0.11 \pm 0.06$ [37]. This correction reduces the neutrino background sample to 24.5 events. After scaling to the data exposure and accounting for statistical error plus uncertainties arising from our atmospheric neutrino MC including the neutrino oscillation correction (see Sect. 7.2), we obtain 4.0 ± 1.0 events as the estimated neutrino-induced background of our $n\bar{n}$ oscillation search.

As discussed in Sect. 3.1, neutron-induced rock events which are background for $n\bar{n}$ oscillations are those which elude tagging by the active shield. As described in Sect. 3.3,

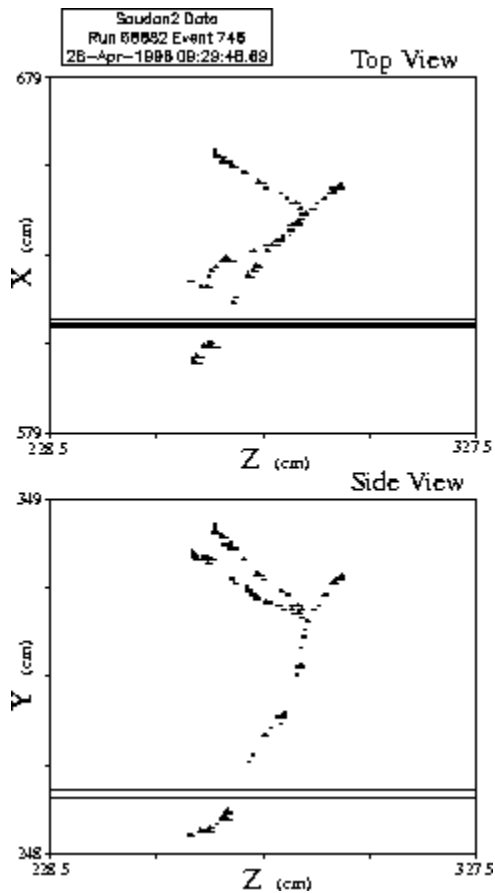


Figure 7: Anode-time and cathode-time views of a four-track $\bar{n}\bar{n}$ oscillation candidate.

we estimate that a fraction $0.06^{+0.11}_{-0.06}$ of data multiprungs are rock events. Thus of the 188 shield-quiet data multiprungs, we estimate $11.3^{+20.6}_{-11.3}$ to be rock events. However, among the 375 shield-tagged rock multiprung events, only fifteen pass our four $\bar{n}\bar{n}$ selection criteria. Thus, assuming that the selection efficiency of shield-quiet rock events is the same as that of shield-tagged rock events, the background of rock events which pass all $\bar{n}\bar{n}$ selections is estimated to be $0.5^{+0.8}_{-0.5}$ events.

In summary, we estimate the number of background events to be 4.0 ± 1.0 (*atm. ν*) plus $0.5^{+0.8}_{-0.5}$ (*rock*) = 4.5 ± 1.2 events.

6 Neutron Oscillation Time Lower Limits

Having observed five candidate $\bar{n}\bar{n}$ oscillation events and having calculated background neutrino and cosmic ray processes to contribute 4.5 events, we set a lower limit for the $\bar{n}\bar{n}$ oscillation time T_A in iron nuclei. We follow previous experiments in using our best estimate of the background in determining the limit. Additional uncertainties in the limit due to the uncertainties in the background calculation are discussed in Sect. 7. We use the approach to confidence level construction as formulated by Feldman and Cousins [38, 39]. For five candidate events with 4.5 background events the signal limit at 90% CL is $n_{90} = 5.5$ events.

$n\bar{n}$ <i>Simulation</i>	T_A <i>lower limit</i>	$\tau_{n\bar{n}}$ <i>lower limit</i>
$n\bar{n}$ without INS	$11. \times 10^{31}$ y	1.6×10^8 s
$n\bar{n}$ in Nuclear Periphery, with INS	8.4×10^{31} y	1.4×10^8 s
$n\bar{n}$ throughout Nucleus, with INS	7.2×10^{31} y	1.3×10^8 s

Table 4: Neutron-antineutron oscillation time lower limits (90% CL) arising from three different treatments of pion intranuclear scattering in $n\bar{n}$ annihilations. Simulations of the second and third rows are regarded to be realistic; the one with more conservative nuclear modelling (bottom row) is the basis for the limits for this search.

The oscillation time lower limit is then calculated using

$$T_A > \frac{N_n \cdot T_f \cdot \epsilon}{n_{90}} \quad (2)$$

Here, $N_n = 3.15 \times 10^{32}$ neutrons in a kiloton of the Soudan 2 detector, $T_f = 6.96$ kiloton years is the full detector exposure, and $\epsilon = 0.18$ is the efficiency for detection of $n\bar{n}$ oscillations in the full detector mass, calculated using our primary $n\bar{n}$ simulation (see Sect. 5). At 90% CL we obtain $T_A > 7.2 \times 10^{31}$ years.

Equation (1) shows that the free $n\bar{n}$ oscillation time $\tau_{n\bar{n}}$ can be inferred from oscillation time T_A for neutrons of nucleus A . For the suppression factor of iron we use the value $T_R = 1.4 \times 10^{23} \text{ s}^{-1}$ obtained by Dover, Gal, and Richard upon averaging over calculations using different nuclear optical potentials [7]. Similar or moderately higher T_R values have been reported from other calculations[8, 11]. At 90% CL we obtain $\tau_{n\bar{n}} > 1.3 \times 10^8$ seconds.

Oscillation time lower limits based upon detection efficiencies of each of our three $n\bar{n}$ simulations are summarized in Table 4. The range of values which results from the variation in ϵ illustrates the important role of the intranuclear rescattering treatment. The alternative simulations serve as estimators of sensitivity to systematic uncertainties arising from modelling of the nuclear environment.

7 Statistical and Systematic Uncertainties

Our lower limits for T_A and $\tau_{n\bar{n}}$ contain uncertainties arising from finite statistics of data and simulation samples and from systematic errors inherent in our analysis techniques. To quantify these uncertainties, we have evaluated the error contributions which enter via each of the factors of Eq. (2).

7.1 Exposure and $n\bar{n}$ detection efficiency

The N_n value [22] and the detector exposure are known accurately, with a consequent fractional error for the factor $N_n \times T_f$ of order 2%.

The $n\bar{n}$ detection efficiency ϵ has statistical error due to the finite sample size of our primary simulation at generation and especially after cuts. Furthermore, systematic uncertainties may arise due to inaccuracies in the simulation. Based upon trial variations of

relative rates among dominant $\bar{n}N$ channels (cross sections known to $\leq 20\%$), we estimate channel rate uncertainties to contribute $\sim 5\%$ uncertainty to ϵ . A systematic error in ϵ may arise from our placement of annihilation sites within parent nuclei. Based upon our alternative simulations, we assign a 17% fractional uncertainty to modelling details. There are uncertainties inherent with our treatment of pion intranuclear rescattering. Compared to the unphysical case wherein INS is neglected, our treatment gives rise to an efficiency decrease $\Delta\epsilon = 0.10$. Uncertainty in the amount of this decrease arises from finite statistics of bubble chamber neutrino samples [29] and with extrapolation from $A = 20$ to 56 of the component INS processes, namely pion absorption, charge exchange, inelastic and elastic scattering. We estimate the latter uncertainties to total 30% [30]. We then infer the fractional error contribution to ϵ arising from our INS treatment to be 17%. Combining the above uncertainties in quadrature, we estimate the total fractional uncertainty $\delta\epsilon/\epsilon$ to be 27%.

7.2 Background estimation

The value of n_{90} relies upon our estimation of rates for background events which satisfy the $n\bar{n}$ oscillation search criteria.

Our estimate of atmospheric neutrino backgrounds is susceptible to errors from three sources: (i) Uncertainty arises from event statistics (after cuts) of the atmospheric neutrino simulation (19%); (ii) The normalization of the ν MC to the experimental exposure, which predicts 183 neutrino events will be observed, is uncertain. From our data we observe (data-rock) = 177 ± 20 events, from which we infer an error (11%). (iii) The atmospheric ν MC may not fully represent aspects of neutrino data which feature in the selections of Sect. 4. However our data imply limits on the extent of MC mis-representation. For data events, and with respect to the cuts applied in Sect. 4, we observe $34 \pm 5\%$ to have $n_{prongs} \geq 4$, $78 \pm 9\%$ to be devoid of protons, $67 \pm 8\%$ to be devoid of “muons”, and $43 \pm 6\%$ to have kinematics in the vicinity ($500 \leq E_{vis} \leq 1800$ MeV, $P/E \leq 0.8$) of our search region. The corresponding fractions for the ν MC sample are 35%, 76%, 64%, and 39% respectively. The agreement is good, and we take the quadrature sum of the fractional differences $|Data - MC|/Data$ in the four ratios as our estimator of uncertainty arising from MC representation of atmospheric neutrino physics (11%). The total fractional error for our atmospheric neutrino background is then 25%, which corresponds to an error of ± 1.0 events on our estimate of 4.0 neutrino-induced background events.

Concerning our estimate of background from rock events, the uncertainty arising from the determination of rock-event contribution to the vertex depth distribution of shield-quiet multiprongs outweighs any other systematic uncertainty.

The total absolute error assigned to our 4.5 background events from atmospheric neutrinos and rock amounts to ± 1.2 events. Variation of our background estimate by $\pm 1 \sigma$ yields $\delta n_{90}/n_{90} = 21\%$. The total uncertainty in our oscillation time lower limit value for T_A thereby implied by Eq. (2) is $\delta T_A/T_A = 34\%$.

Our limit for the oscillation time of free neutrons $\tau_{n\bar{n}}$ depends upon the nuclear suppression factor T_R as implied by Eq. (1). For T_R of iron, we used the value of Dover *et al.* [7], $T_R = 1.4 \times 10^{23} \text{ s}^{-1}$. However from the range of T_R ($A=56$) values indicated by the calcula-

<i>Experiments</i>	<i>Source of neutrons</i>	<i>Exposure fiducial (total)</i> kton-years	<i>Cand. Events</i>	<i>Est. Bkgrd</i>	T_R	T_A	$\tau_{n\bar{n}}$
					10^{23} s^{-1}	10^{31} y	10^8 s
Grenoble('90) [15]	reactor beam	-	0	0	-	-	0.86
Kamiokande('86) [20]	^{16}O	1.11	0	1.2	1	4.3	1.2
Fréjus('90) [21]	^{56}Fe	1.56 (2.56)	0	2.5,2.1	1.4	6.5	1.2
Soudan 2 [this study]	^{56}Fe	5.56 (6.96)	5	4.5	1.4	7.2	1.3

Table 5: Experimental lower limits at 90% CL for $n\bar{n}$ oscillation times T_A and $\tau_{n\bar{n}}$ of bound and free neutrons respectively. For results of this search (bottom row), the background estimate is corrected for $\nu_\mu \rightarrow \nu_\tau$ oscillations and limits are calculated using the Feldman-Cousins method.

tion of Alberico *et al.* [11], a theoretical uncertainty as large as 100% may be inferred. Then the fractional error in $\tau_{n\bar{n}}$ is $\delta\tau_{n\bar{n}}/\tau_{n\bar{n}} \approx 53\%$.

We conclude that the uncertainties $\delta T_A/T_A$ and $\delta\tau_{n\bar{n}}/\tau_{n\bar{n}}$ on the oscillation time lower limits obtained in this work may be as large as 34% and 53% respectively. Of course, comparable uncertainties also apply to other published limits on $n\bar{n}$ oscillation times.

8 Comparison with Previous Experiments

Table 5 compares our results with those obtained by the three most recent of previous searches. The numbers of candidate events and corresponding estimates for background rates are shown in columns four and five. Background estimates for the underground experiments (1.1, 2.5, 4.5 events for Kamiokande, Fréjus, and Soudan 2 respectively) are based upon simulations of atmospheric neutrino interactions in the detectors. For the Fréjus experiment, an alternative estimate of 2.1 background events was obtained based upon interactions recorded using planar spark chambers exposed to beams of neutrinos and antineutrinos at the CERN-PS [40]. Soudan 2 is the underground experiment with the largest exposure. It is also the only experiment to observe candidate events, although all of the underground experiments estimated about one background event per kiloton year.

A degree of caution is warranted when comparing oscillation time lower limits for free neutrons as calculated by underground experiments versus a reactor neutron beam experiment (last column of Table 5). The $\tau_{n\bar{n}}$ limits of Soudan 2, Fréjus, and Kamiokande are based upon values for the neutron suppression factor T_R as calculated by Dover *et al.* [7]. However if T_R values for iron and oxygen are considered which are at the high end of ranges obtained by Alberico *et al.* [11], then limits at or below the Grenoble value are implied for the underground experiments.

9 Summary And Conclusion

The fine-grained Soudan 2 tracking calorimeter has been used in a search for neutron-to-antineutron oscillations occurring with bound neutrons. Based upon a fiducial exposure of

5.56 kiloton-years of the underground detector, a new oscillation time lower limit for $n\bar{n}$ oscillations in iron nuclei has been determined at 90% CL:

$$T_A (Fe) > 7.2 \times 10^{31} \text{ y.} \quad (3)$$

Assuming the suppression factor for iron is $T_R = 1.4 \times 10^{23} \text{ s}^{-1}$ [7], the corresponding limit at 90% CL for n to \bar{n} oscillations of free neutrons is

$$\tau_{n\bar{n}} > 1.3 \times 10^8 \text{ s.} \quad (4)$$

The search reported here is background-limited. Candidate events are observed to occur at a rate similar to that predicted for backgrounds. Since the predominant background arises from kinematic overlap with multiprong reactions initiated by atmospheric neutrinos, it seems unlikely that future underground experiments can avoid also becoming background-limited in larger exposures. Thus reactor neutron beam experiments, rather than underground experiments monitoring bound neutrons, may offer a more promising route for future improvements in sensitivity to $\tau_{n\bar{n}}$ (see [41] and references therein).

Acknowledgements

This work was supported by the U.S. Department of Energy, the U.K. Particle Physics and Astronomy Research Council, and the State and University of Minnesota. We gratefully acknowledge the Minnesota Department of Natural Resources for allowing us to use the facilities of the Soudan Underground Mine State Park.

References

- [1] V.A. Kuzmin, JETP Lett. **12**, 228 (1970).
- [2] A.D. Sakharov, JETP Lett. **5**, 24 (1967).
- [3] R.N. Mohapatra and R.E. Marshak, Phys. Rev. Lett. **44**, 1316 (1980); Phys. Lett. **94B**, 183 (1980); L.-N. Chang and N.-P. Chang, Phys. Lett. **92B**, 103 (1980); T.K. Kuo and S. Love, Phys. Rev. Lett. **45**, 93 (1980); R. Cowsik and S. Nussinov, Phys. Lett. **101B**, 237 (1981); S. Rao and R. Shrock, Phys. Lett. **116B**, 238 (1982); Nucl. Phys. **B232**, 143 (1984).
- [4] Z. Chacko and R.N. Mohapatra, Phys. Rev. D **59**, 055004 (1999); K. S. Babu and R. N. Mohapatra, Phys. Lett. B **518**, 269 (2001).
- [5] Stephan J. Huber and Qaisar Shafi, Phys. Lett. B **512**, 365 (2001); S. Nussinov and R. Shrock, Phys. Rev. Lett **88**, 171601 (2002).
- [6] W. M. Alberico, *in*: Proceedings of the Workshop on Future Prospects of Baryon Instability Search in p-Decay and N- \bar{N} Oscillation Experiments, ed. S.J. Ball and Y. A. Kamyshev, ORNL-6910, March 1996; pp. 221-234.

- [7] C.B. Dover, A. Gal and J.M. Richard, Phys. Rev. D **27**, 1090 (1983); Phys. Rev. C **31**, 1423 (1985); Nucl. Instr. Meth. A **284**, 13 (1989).
- [8] J. Huefner and B.Z. Kopeliovich, Mod. Phys. Lett. A **13**, 2385 (1998).
- [9] K.G. Chetyrkin, M.V. Kazarnovsky, V.A. Kuzmin, and M.E. Shaposhnikov, Phys. Lett. **99B**, 358 (1981).
- [10] W.M. Alberico, A. Bottino and A. Molinari, Phys. Lett. **114B**, 266 (1982); W.M. Alberico, J. Bernabeu, A. Bottino and A. Molinari, Nucl. Phys. A **429**, 445 (1984).
- [11] W.M. Alberico, A. De Pace and M. Pignone, Nucl. Phys. A **523**, 488 (1991).
- [12] L.A. Kondratyuk, JETP Lett. **64**, 495 (1996).
- [13] G. Bressi *et al.*, Z. Phys. C **43**, 175 (1989).
- [14] G. Fidecaro *et al.*, Phys. Lett. **156B**, 122 (1985).
- [15] M. Baldo-Ceolin *et al.*, Phys. Lett. B **236**, 95 (1990); Z. Phys. C **63**, 409 (1994).
- [16] Homestake Collaboration, M. L. Cherry *et al.*, Phys. Rev. Lett. **50**, 1354 (1983).
- [17] NUSEX Collaboration, G. Battistoni *et al.*, Phys. Lett. B **133**, 454 (1983).
- [18] KOLAR Collaboration, M.R. Krishnaswamy *et al.*, Nuovo Cim. C **9**, 167 (1986).
- [19] IMB Collaboration, T.W. Jones *et al.*, Phys. Rev. Lett. **52**, 720 (1984).
- [20] Kamiokande Collaboration, M. Takita *et al.*, Phys. Rev. D **34**, 902 (1986).
- [21] Fréjus Collaboration, Ch. Berger *et al.*, Phys. Lett. B **240**, 237 (1990).
- [22] Soudan 2 Collaboration, W.W.M. Allison *et al.*, Nucl. Instr. Meth. A **376**, 36 (1996); Nucl. Instr. Meth. A **381**, 385 (1996).
- [23] Soudan 2 Collaboration, W.P. Oliver *et al.*, Nucl. Instrum. Methods Phys. Res. A **276**, 371 (1989).
- [24] Soudan 2 Collaboration, D. Wall *et al.*, Phys. Rev. D **62**, 092003 (2000).
- [25] A. Bodek and J.L. Ritchie, Phys. Rev. D **23**, 1070 (1981).
- [26] R.B. Chaffee, SLAC Computation Group Technical Memo No. 195, 1979.
- [27] G. Backenstoss *et al.*, Nucl. Phys. B **228**, 424 (1983). A convenient compilation of channel rates based on this work appears in Yu.A. Golubkov and M.Yu. Khlopov, astro-ph/0005419; submitted to Yad. Fiz.

- [28] N. Horwitz *et al.*, Phys. Rev. **115**, 472 (1959); R. Armenteros and B. French, *in*: High Energy Physics, edited by E.H.S. Burhop (Academic, New York, 1969), Vol. 4, p. 237; C. Ghesquiere, *in*: Proceedings of the Symposium on Antinucleon-nucleon Interactions, Liblice-Prague, Edited by L. Montanet, CERN 74-18, (1974), p. 436; P. Pavlopoulous *et al.*, *in*: Nucleon-Nucleon Interactions 1977, Proc. of the Second Int. Conf., Vancouver, Edited by H. Fearing, D. Measday, and A. Strathdee (AIP Conf. Proc. No. 41), (AIP, New York, 1978), p. 340.
- [29] R. Merenyi *et al.*, Phys. Rev D **45**, 743 (1992).
- [30] Soudan 2 Collaboration, D. Wall *et al.*, Phys. Rev. D **61**, 072004 (2000).
- [31] Soudan 2 Collaboration, W.W.M. Allison *et al.*, Phys. Lett. B **427**, 217 (1998); see Sect. 3.2.
- [32] V. Agrawal, T.K. Gaisser, P. Lipari, and T. Stanev, Phys. Rev. D **53**, 1313 (1996).
- [33] H.R. Gallagher, Ph.D. thesis, University of Minnesota, 1996; H. Gallagher and M. Goodman, Soudan 2 internal note PDK-626 (MINOS note NuMI-L-112), 1995(unpublished).
- [34] M. Derrick *et al.*, Phys. Rev. D **30**, 1605 (1984).
- [35] Super-Kamiokande Collaboration, Y. Fukuda *et al.*, Phys. Lett. B **433**, 9 (1998); Phys. Rev. Lett. **81**, 1562 (1998); Phys. Lett. B **436**, 33 (1998); Phys. Rev. Lett. **85**, 3999 (2000).
- [36] MACRO Collaboration, S. Ahlen *et al.*, Phys. Lett. B **357**, 481 (1995); M. Ambrosio *et al.*, Phys. Lett. B **434**, 451 (1998); Phys. Lett. B **478**, 5(2000); Phys. Lett. B **517**, 59 (2001).
- [37] Soudan 2 Collaboration, W.A. Mann, Nucl. Phys. B (Proc. Suppl.) **91**, 134 (2001).
- [38] G. J. Feldman and R. D. Cousins, Phys. Rev. D **57**, 3873 (1998).
- [39] Particle Data Group, Eur. Phys. J. C **15**, 201 (2000).
- [40] Fréjus Collaboration, Ch. Berger *et al.*, Nucl. Instr. Meth. A **302**, 406 (1991).
- [41] Yu. Kamyshkov, “Nucleon Instability and ($B-L$) Non-Conservation”, *in*: Proc. NNN99 Workshop, AIP Conf. Proc. 533, Edited by M.V. Diwan and C.K. Jung, Stony Brook, New York, September 1999; p. 84.